



Identification of Flow Physics in a Counter Rotating Turbine

R. Subbarao[†] and M. Govardhan

Department of Mechanical Engineering, Indian Institute of Technology Madras, Chennai, 600036, India

[†]*Corresponding Author Email: rsubbarao@hotmail.com*

(Received April 1, 2019; accepted August 19, 2019)

ABSTRACT

Flow in a Counter Rotating Turbine (CRT) stage is composite and three dimensional due to the blade geometry of nozzle, rotor 1 and rotor 2 that are twisted along the span, spacing between them, tip clearance provided on rotors and also because of oppositely rotating rotors. Present work analyzes the flow field through the nozzle and rotors at planes taken at various axial chord distances. Blade-to-blade contours and the hub-to-tip plots reveal the actual scenario of flow in the turbine stage. Nozzle and the two rotors are modeled in case of the CRT configuration. Boundary conditions are specified as pressure at inlet of the nozzle and flow rate at the outlet of rotor 2. Total pressure, velocity, entropy and TKE distribution through the blades are used to identify the flow over CRT. Flow through the blade rows is distinguished by effects of boundary layer, secondary flows near the hub, pressure gradient effects, presence of vortical flow structures in the passage and near the tip. Total pressure distribution near the midspan in case of nozzle and rotors show the presence of boundary layers and wake regions. Entropy and TKE contours show the loss regions in all the blade rows. Flow losses are more in rotor 2 than rotor 1. Secondary velocity vectors show the presence of vortex regions in the passage and tip clearance. Blade-to-blade contours of CRT reveal the actual flow scenario surrounding the blades. Hub-to-tip plots show the variations of flow parameters while moving from the bottom to top most position of blade. Thus, the present work identifies the exact flow structure in a counter rotating turbine and paves the way for researchers to negotiate flow losses and improve the CRT performance further.

Keywords: Counter Rotating Turbine (CRT); Blade-to-Blade contours; Hub-to-Tip plots; Vortices; Flow losses.

NOMENCLATURE

a	axial chord	s	blade spacing
CRT	Counter Rotating Turbine	SS	Suction Surface
LE	Leading Edge	TV	tip side vortex
PS	Pressure Surface	TE	Trailing Edge
PV	Passage Vortex	TKE	Turbulent Kinetic Energy
r/r_t	Radius normalized by tip radius	x, y	distance along x and y - axes

1. INTRODUCTION

Gas turbine technology has steadily advanced since its inception and research carried till now led to the improvement in performance thus reducing the cost. It is estimated that just 1% improvement in the efficiency of the turbine in commercial aircraft engines would save cost depending on the application and usage. Thus, it has been the prime interest of the researchers to investigate their

performance by analyzing the nature of the complex flow in a turbine. Axial turbine consists of nozzles and rotors subsequently positioned in the stream pathway. Stationary guide vanes accelerate the flow in the required direction and moving blades convert the pressure and kinetic energy of the fluid into mechanical work on the shaft. Growing concern for efficiency rise and reduction of weight in aero engines lead to an alternative turbine that has two rotors. In case of counter rotating turbine (CRT),

nozzle is followed by two rotors that rotate in the reverse direction of each other. Due to the exceptional architecture and nonexistence of the subsequent nozzle, flow in a CRT stage is complex and three-dimensional. Flow interaction between the stationary nozzle and rotor 1 as well as rotor 1 and rotor 2 further add to the complexity of the flow. Earlier, [Wintucky and Stewart \(1957\)](#) and [Louis \(1985\)](#) showed that such turbines could ensure better performance than the conservative turbines. [Ozgun and Nathan \(1971\)](#) deliberated CRT stage that has equivalent speeds and definite work in both the blades. Their analyses provided more details about CRTs with little or no guidance for the practical design. [Ji et al. \(2001\)](#) explored the workability of CRT and found specific work ratio and flow angle as important parameters.

[Zhao et al. \(2007\)](#) numerically studied the three dimensional flow in a vaneless counter rotating turbine for various tip clearances. The comparison of conventional and counter rotating turbines with respect to essential and thorough performances for different stages was presented by [Moroz et al. \(2009\)](#). Steps of aerodynamic design of CRT, optimization and off-design performance estimation were described. Work done by the same authors ([Subbarao and Govardhan \(2014\)](#)) studied the effect of speed ratio on the performance of a counter rotating turbine. But, flow aspects through the turbine blade rows are not discussed. It is found that none of these works described the flow pattern through the CRT stage. In this context, present work finds significance with the modelling and simulation of CRT blade rows with respect to the identification of flow. Study carried out in this paper will be useful for the gas turbine community to reduce flow losses and improve stage performance.

2. METHODOLOGY

CRT considered in this study has 22, 28 and 28 blades of nozzle, rotor 1 and rotor 2 respectively. ANSYS® ICEM CFD 14.0 is used for modeling and meshing of the turbine components. As shown in Fig. 2, computational model of CRT contains the blade rows of nozzle and the two rotors. Table 1 shows the revised blades profile details of the nozzle and rotors acquired from [Dring et al. \(1987\)](#). On both the rotors, 2.28 mm tip clearance is provided. Table 2 shows the details of nozzle and rotor profiles at the midspan section. Same profile is used for both the rotors. The axis of revolution is X-axis. Periodic flow is considered here in case of all the blades. In order to keep pitch ratio about 1, three blades of nozzle and four blades of the rotors are considered. For mesh generation, Tetra meshing is used. It provides a robust smoothing procedure for mesh refinement. Prism meshing is considered with layers near the boundary surfaces for better prediction of the flow close to the wall. Mesh distribution is done with more elements adjoining the blade, LE and TE as showed in Fig. 3 for nozzle. Capturing of the edges and the growth of the mesh from walls to the blade and the interior

zone has been excellent as seen in the nozzle mesh. Similar technique is used for rotor 1 and rotor 2 also.

At nozzle inlet, stagnation pressure is taken as boundary condition. At rotor 2 outlet, mass flow rate is specified. Table 3 shows the details of flow parameters and values of axial gaps, speed ratios and stagger angles. The working fluid is considered as air ideal gas. Frozen rotor is used for rotor-stator frame change interface. Rotational speed of the rotors is 600 RPM. Rotor 1 rotates in the clockwise direction when observed from the upstream of the rotor. Rotor 2 rotates with the same speed, but in the anti-clockwise direction, opposite to the first rotor. Based on the inlet boundary condition, turbulence intensity of the incoming flow is considered as 1% for all the configurations. Reference pressure is taken as 1 atm. Convergence criteria of target RMS residual value is set as 10^{-4} . Regular turbulence model Shear Stress Transport (SST) built on $k-\omega$ is considered.

Table 1 CRT blade configuration

Parameter	Nozzle	Rotor 1	Rotor 2
Number of blades	22	28	28
Hub radius (mm)	610	610	610
Tip radius (mm)	762-776	776-790	790-805
Tip clearance (mm)	0	2.28	2.28

Table 2 Details of nozzle and rotor profiles at the midspan section

Details	Nozzle	Rotor
Axial chord (mm)	151	116
Blade spacing (mm)	195.11	154.9
Space-chord (s/ch) ratio	0.85	0.85
Blade inlet angle	90°	138°
Blade exit angle	21.42°	25.97°
Stagger angle	49.56°	31.59°
Deflection angle	68.58°	111.85°

Table 3 Simulation parameters used

Parameter	Value
Temperature at inlet (K)	480
Inlet total pressure (Pa)	1.35×10^5
Equivalent flow rate	0.091 - 0.137
Working fluid	Air ideal gas
Inlet turbulence (%)	1

3. PRELIMINARY STUDIES

Mesh independence study is carried out in order to see that the results are not dependent on the mesh. This study is performed by altering the number of mesh elements with the help of global mesh parameter variation. Pressure coefficient on the blade is calculated by obtaining the pressure at all the locations of pressure and suction sides of the blade. Figure 3 shows the pressure coefficient values of rotor for four mesh sizes of 3.0 to 4.1 millions. The trend showed similar pattern as that of nozzle. As the mesh size is increased from 3.0 to 3.6 millions, pressure coefficient is observed as increasing. As the mesh size is raised further, pressure coefficient of the rotor remained constant. Hence, in case of rotor, the optimized mesh of 3.6 million elements is chosen, as there is no variation of the measured variable further with change in mesh size. This also ensures that computational time is saved and flow physics is accurately captured. Similarly, an optimized mesh of 3.7 million is chosen for nozzle and mesh of 5.4 million is chosen for rotor 2. Thus, mesh independence study takes care of the optimized mesh size, computational time and variation of selected flow or performance variable.

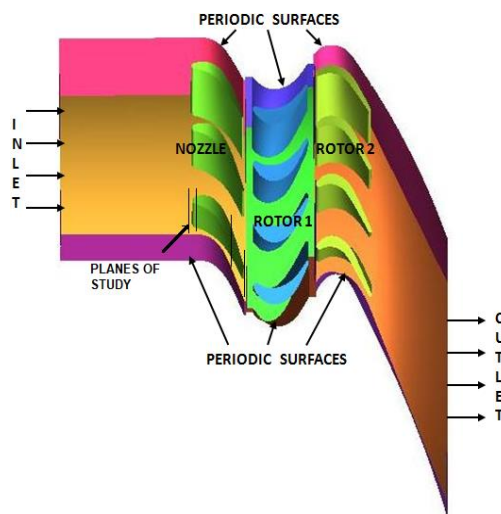


Fig. 1. Computational domain of CRT.

Similarly, in case of other blades, optimized mesh is chosen such that there is no variation of the measured variable further with change in mesh size. Computational results are verified with the results obtained on a rotating turbine rig by Dring *et al.* (1987). As presented in Fig. 4, pressure on rotor blade is used for comparison. It is obtained from the change in blade surface and reference pressures at blade inlet. Normalization is done by the inlet total pressure. Pressures from simulation are in decent agreement except for a small region near the trailing edge. The slight deviation near the leading is due to over prediction of simulation results. Near the trailing edge, it may be due to the variation in capturing the minute edges by

computational model.

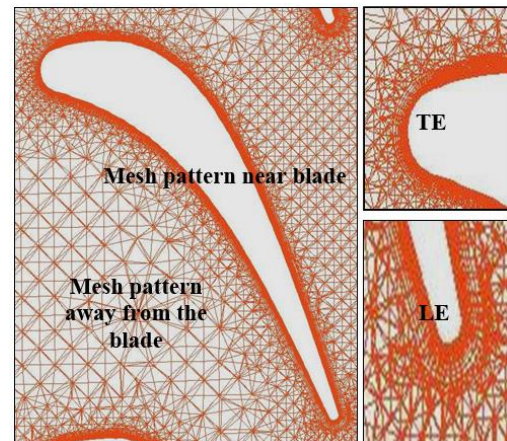


Fig.2. Mesh for the nozzle blade.

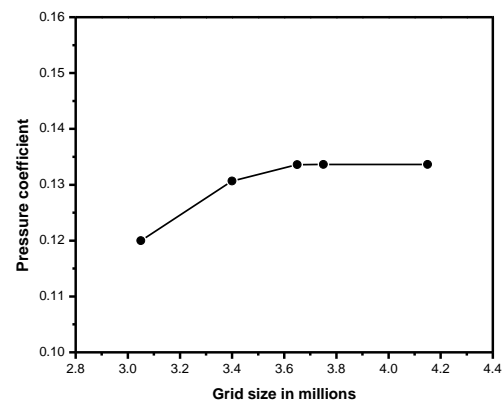


Fig. 3. Mesh independence study details of rotor.

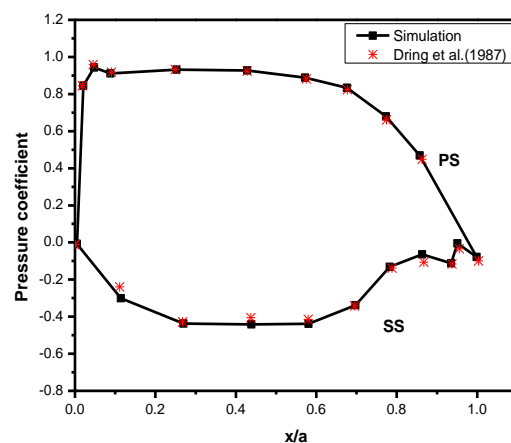


Fig. 4. Pressure coefficient of rotor blade at midspan.

4. RESULTS AND DISCUSSION

Flow through the CRT stage is complex and the aim of the current work is to present and analyze the features of flow field in nozzle, rotor 1 and rotor 2 that affect its performance. Total pressure, velocity, entropy and Turbulent Kinetic Energy (TKE) are considered as parameters to describe the flow. Total

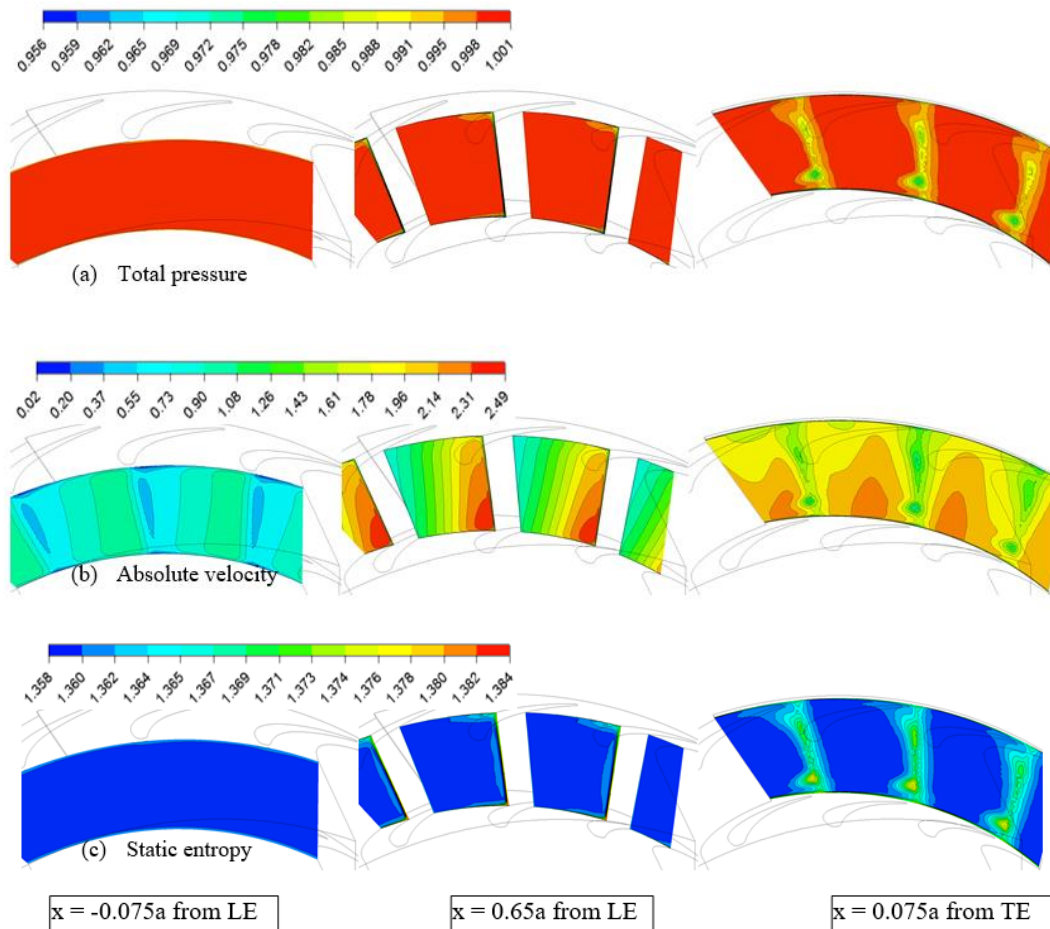


Fig. 5. Total pressure, velocity and entropy through nozzle at various planes.

pressure at inlet of the turbine is used to normalize pressures. Velocities are normalized by tip blade speed. Gas constant is used to normalize entropy. Normalization of TKE is done with the square of velocity. These parameters are plotted at planes before LE (-0.075a) and after LE (0.02a), just after mid-chord (0.65a) and just after TE (0.075a). Planes are taken at half the axial gap distance, before and after the blade rows. Blade-to-blade contours, hub-to-tip plots and contours drawn along the transverse plane reveal the actual scenario of the flow in the turbine stage.

4.1 Flow Through Nozzle

Present section analyzes the flow field through the nozzle, rotor 1 and rotor 2 at various planes along the chord. For Nozzle, three planes are taken, one before the leading edge and another one after the trailing edge of the blade at a distance of 7.5% of the chord. Third plane is taken at 65% of the axial chord distance. Figure 5 (a) displays the total pressure distribution along the nozzle blade passage. At the inlet plane, before the leading edge, total pressure remains constant. As the flow passes through the nozzle, hub and tip side secondary losses are observed on suction side after the mid-chord section. These are recognized at the

blade span of 20% besides 80%. At the exit of the nozzle vane, clear and distinct wake region is observed. Hub and tip side vortices are observed with difference in strength and shape. Pressures are low in the wake and vortex regions. At the inlet of the nozzle, velocities are low and clearly distinctive pattern is observed near the leading edge as shown in Fig. 5 (b). Further downstream, velocities on the pressure side region continue to be low, whereas, on the suction side there is sudden increase in velocity after LE, followed by acceleration. Velocity distribution near the trailing edge supports the pattern described in the total pressure contours shown. Velocities are low in the core region of the wake. Overall, the absolute velocity is increasing from nozzle inlet to outlet. Entropy contours through the nozzle vane at various locations are shown in Fig. 5 (c). Up to the mid-chord section of the nozzle, entropy values are less. As the flow moves further, entropy increases in the downstream of the blade near the endwalls. Entropy generated on the suction side region is high compared to that on the pressure side from the throat section because of pressure gradients. Near the hub and tip, losses spread due to the boundary layer effect, which can be observed in the entropy distribution drawn on the planes just after the trailing edge of the vane.

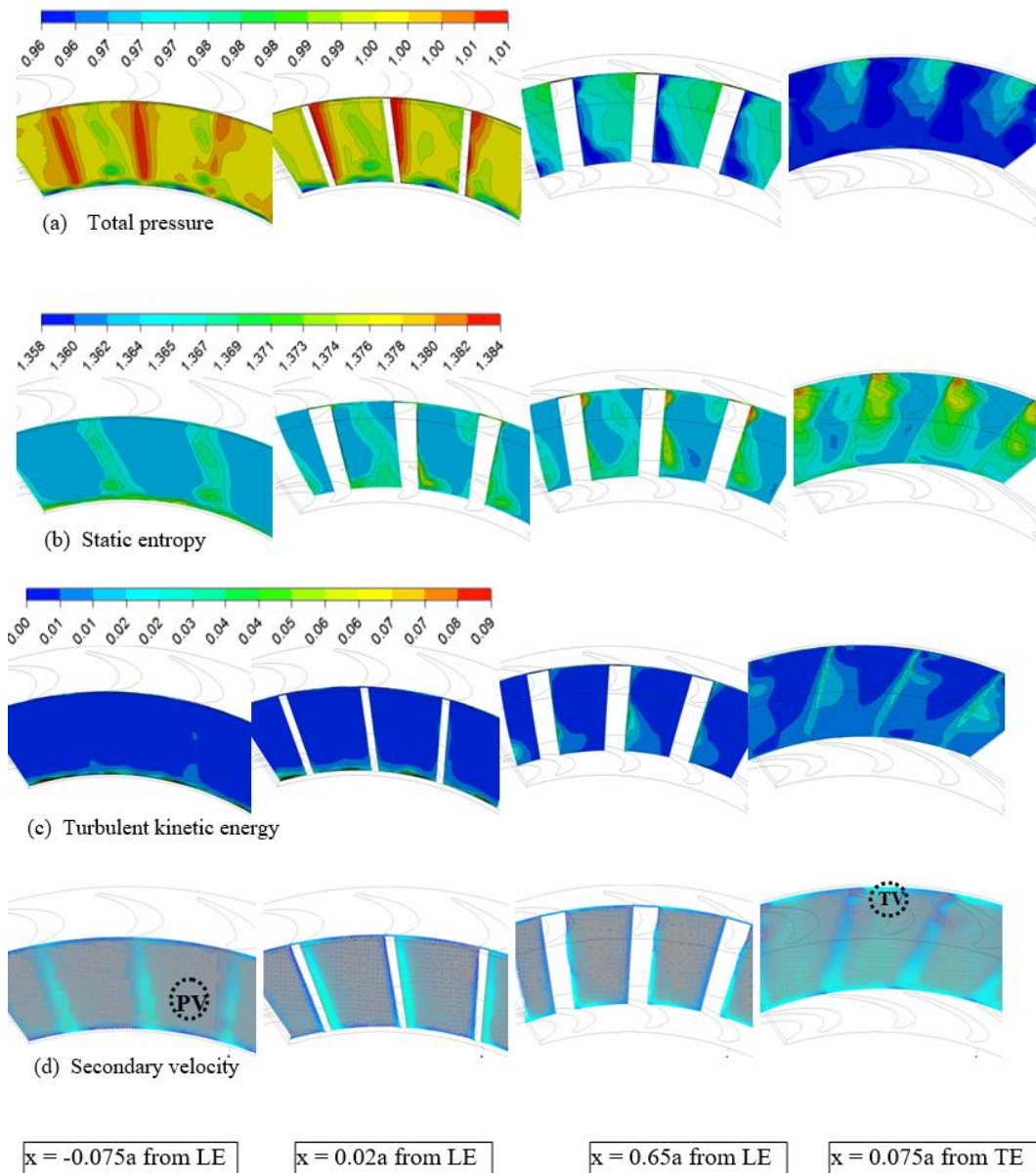


Fig. 6. Total pressure, entropy, TKE and secondary velocity vectors from inlet to outlet of rotor 1 at various planes.

4.2 Flow Through Rotor 1

Total pressure from inlet to outlet of rotor 1 at various planes is shown in Fig. 6 (a). Apart from the three planes taken as in case of nozzle, additional plane at a distance of 2% chord is considered in rotors to get clearer picture of the flow just after contacting with the moving blade. Total pressure values are highest near the leading edge as the flow from nozzle interacts rotor 1 with less incidence. As the flow passes through the rotor, hub and tip side pressures reduce on the suction side region. Low pressures along the span on SS after mid-chord is a result of grown hub and tip secondary flows. Near the hub, these flows move radially outward and near the tip, are radially inward. On the pressure side region, pressure variation is less throughout the span. Total pressure change in rotor signifies the conversion of energy in rotor. Entropy from inlet to

outlet of rotor 1 at various axial planes is revealed in Fig. 6 (b). Entropy features of nozzle flow exit field are carried to the inlet of the rotor in the form of wake losses that are observed near the leading edge. Secondary flow losses near the hub are also observed initially in rotor 1 passage. As the flow passes further, after the mid-chord region, entropy on the suction side increases. Tip clearance loss is observed to be more when compared to the passage losses as entropy values are more near the tip region. It is also seen that tip clearance and passage losses grow together near the trailing edge of the rotor 1. Entropy values are more in the rotor region compared to the nozzle, which is due to the rotational effects. Overall entropy rise is observed from rotor 1 inlet to outlet.

TKE variation in rotor 1 at various axial planes is observed as shown in Fig. 6 (c). At the plane before

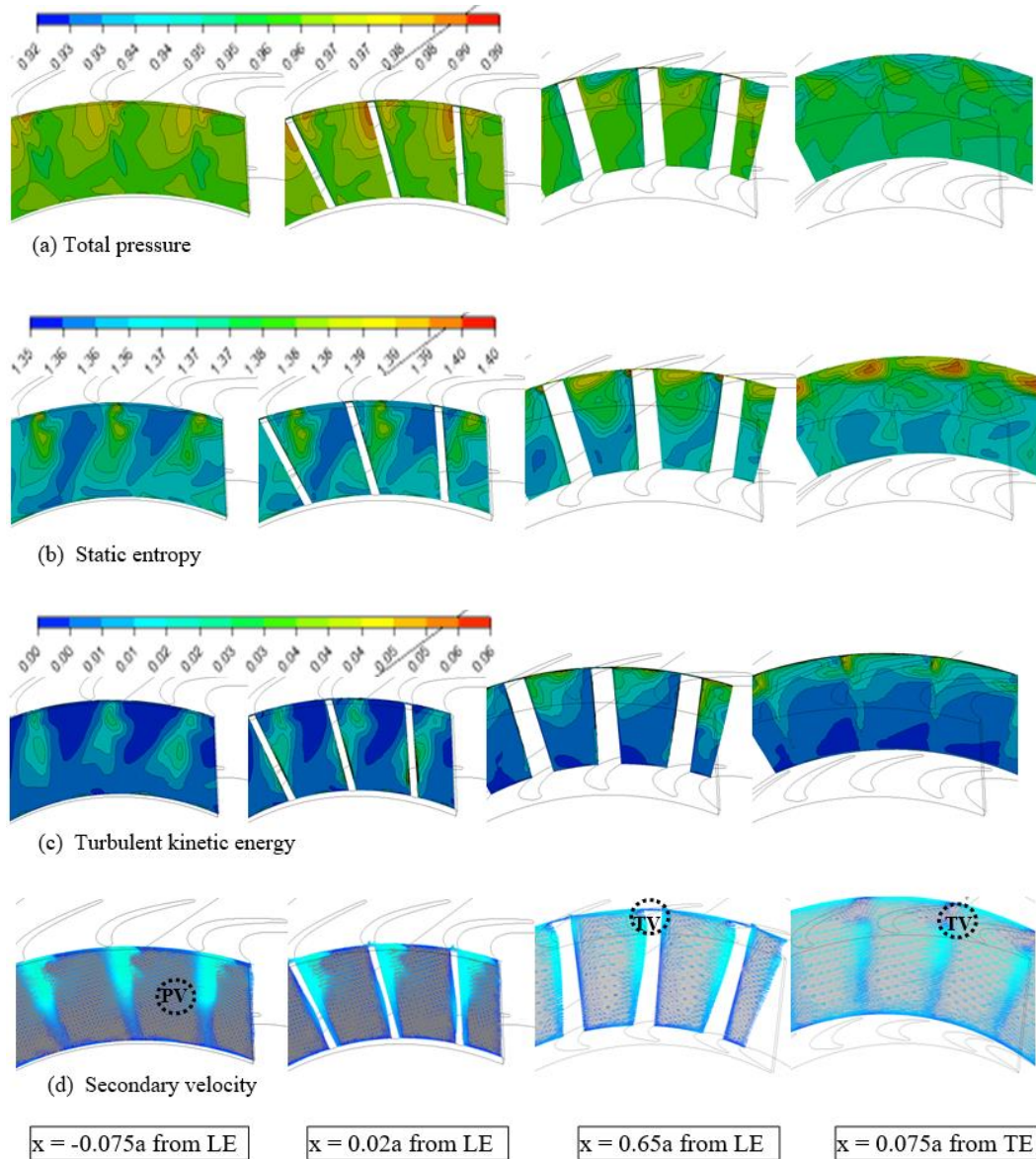


Fig. 7. Total pressure, entropy, TKE and secondary velocity vectors from inlet to outlet of rotor 2 at various planes.

the LE of the rotor 1, higher TKE is observed near the hub as flow comes in contact with rotor 1 as shown in the contour drawn before the leading edge. As the flow passes through the passage, TKE along the suction side of the blade increases, which proceeds to the midspan section. Further, TKE increases as the flow accelerates while travelling to the downstream. TKE observed near the endwall is due to the boundary layer development. Pattern of TKE from inlet to outlet is in corroboration with the movement of the passage vortex. Figure 6 also represents the secondary velocity vectors that show the secondary nature in the flow while passing through rotor. Hub side secondary flow is captured in the planes near the leading edge. Afterwards, passage vortex is observed. As the flow passes further downstream, it gets mixed with the flow. Tip clearance vortex is observed in the planes before and after the trailing edge.

4.3 Flow Through Rotor 2

Total pressure from inlet to outlet of rotor 2 at various planes is shown in Fig. 7 (a). Total pressures are maximum near the LE of rotor 2. As the flow passes through the rotor, pressures reduce steadily towards the trailing edge on the pressure side region. On the suction side, high pressure region is observed just after the flow passes through LE. Further downstream of the flow, pressures are low near the tip wall in the middle of the blade passage. This pattern is continued till the TE of the blade. Overall, total pressure change from inlet to outlet in rotor 2 is less than that of rotor 1. Entropy contours at various axial planes from the inlet to the outlet of the second rotor are shown in Fig. 7 (b). Loss region is spread along the flow passage except at the hub. As the flow passes further in the rotor, high entropy region is found just above the midspan on the pressure side, which tends to move towards

the tip. Entropy contours on the planes near the trailing edge region suggest that losses are highly concentrated in the tip region. This is not observed in case of rotor 1, where passage and tip side losses are combined.

High TKE is observed at the inlet of rotor 2, which is not the case with first rotor as shown in Fig. 7 (c). This is due to the absence of the second guide vane, because of which flow enters rotor 2 with more turbulence. Further downstream of rotor 2, TKE is observed to be more in the tip side region. Below the midspan, TKE is found to be less. When compared to the first rotor, TKE is more in case of the second rotor. At the exit of the CRT stage, tip side flow is more turbulent than the rest of the passage. Flow near the inlet of second rotor signifies the counter rotating stage aspect as the flow is with high velocity and turbulence along with the presence of combined passage and tip side flow losses. This is certainly due to the absence of guide vane, which is not observed at the inlet of the first rotor. Figure 7 (d) describes the secondary velocity vectors in rotor 2 from inlet to outlet. Flow is more of secondary in nature when compared to rotor 1 that is observed throughout the span, starting from the inlet of rotor 2. This tendency is more in rotor 2 up to the mid-chord region, which is because of the flow through the suction zone created between the oppositely rotating blades. Passage vortex observed is large in size and dominant when compared to the first rotor. Tip clearance effect is observed in the plane of $x/a = 0.65$ itself and grows further till the rotor 2 outlet plane.

4.7 Blade-to-Blade Contours of CRT

In this section, Blade-to-blade contours of flow parameters are given that show the inlet to outlet variation in the counter rotating turbine stage for the flow rate of 0.108. These contours give an idea of how parameters change across the blades near the midspan of the passage. Total pressures decrease from inlet to outlet of the turbine as shown in Fig. 8 (a). In nozzle, total pressure variation is less. Pressure losses get initiated near the trailing edge because of the wake formation and get convected to the rotor 1 passage. Pressure varies steadily on the pressure side region in rotor 1. On the suction side, pressure changes are rapid. Fluid in the low pressure region is observed near the leading edge of rotor 2 that affects its performance. On the suction side of the second rotor, pressure increases up to mid-chord section, after which there is no distinctive variation. The pattern of variation of pressure along the streamline in rotor 2 is very different from rotor 1.

Absolute velocity distribution through the turbine stage is shown in Fig. 8 (b). In nozzle, on pressure region, flow rushes effortlessly from LE to TE. On the suction side, there is an overspeed near LE, followed by acceleration. From throat, flow slows down easily to LE. Velocity reduces rapidly on the suction side of rotor 1, due to the pressure changes and flow will turn more following the blade profile. On the pressure side region, velocity reduces steadily till the trailing edge of the blade. Fluid with

low velocity, which is in the wake region of rotor 1 gets convected into the passage of rotor 2. On the pressure side, velocities do not vary much as seen in the Blade-to-blade contour. On the suction side, velocity is maximum up to the mid-chord section, after which, deceleration is observed till the trailing edge. Entropy plots give the extent of losses and how they spread in the turbine stage. In stationary and rotating domains, entropy generation comes from the blade boundary layer and profile losses as well as the wake generation regions. Entropy generation in the passage is observed clearly at nozzle exit TE in wake form, as shown in Fig. 8 (c). Wake is the region of disturbed flow in the downstream of a vane that spreads outward. Entropy variation in nozzle is comparably less as boundary layer losses are observed near the trailing edge section on the suction surface. Further, as the flow moves from nozzle to rotor 1, because of the rotational effects, entropy increases till TE on the pressure side region. On the suction side, entropy increases from the mid-chord region to the trailing edge. Entropy is more on suction side than the pressure side that is attributed to pressure changes and flow following the blade profile. Further, fluid in the high entropy region enters rotor 2. On the pressure side, near LE, losses are more concentrated due to counter rotational effects. On the suction side, entropy variation is less. Entropy values are more in rotor 2 when compared to rotor 1. TKE levels are negligible throughout the first half of the CRT stage as shown in Fig. 8 (d). TKE is slightly more in the Nozzle wake region. In rotor 1, TKE increases from the mid-chord region to the trailing edge on the suction side region. High TKE is observed near the LE of rotor 2 as fluid from rotor 1 enters the zone of two oppositely rotating blades. On the pressure side region, fluid is more turbulent when compared to the suction side. It is clear that TKE convected from the passage of rotor 1 is affecting the performance of rotor 2. As seen in the Figs. 8 (c) and (d), fluid with more entropy and TKE is entering rotor 2, which may adversely affect its performance.

4.7 Hub-to-Tip Variation

In this section, hub-to-tip deviation of total pressure and entropy with mass flow rate is described. These plots show the nature of the flow over the span with circumferential averaging of parameters and are useful in judging the three dimensionality at the entrance and exit of blade rows. Total pressure distribution from hub-to-tip at the inlet and outlets of nozzle, rotor 1 and rotor 2 with respect to change in flow rate is shown in Fig. 9. Similar pattern is detected for all flow rates throughout the turbine passage, where total pressures are decreasing with flow rate. At the entrance and exit of nozzle, total pressures are low near the hub and tip, compared to the rest of the span. At nozzle inlet, total pressure from hub-to-tip is not changing with flow rate as shown in Fig. 9 (a). At nozzle outlet, pressure loss at the hub is changing more with flow rate and less at the tip as shown in Fig. 9 (b). Hub side secondary losses continue to be more at the inlet of rotor 1 when compared to the exit of the nozzle as shown

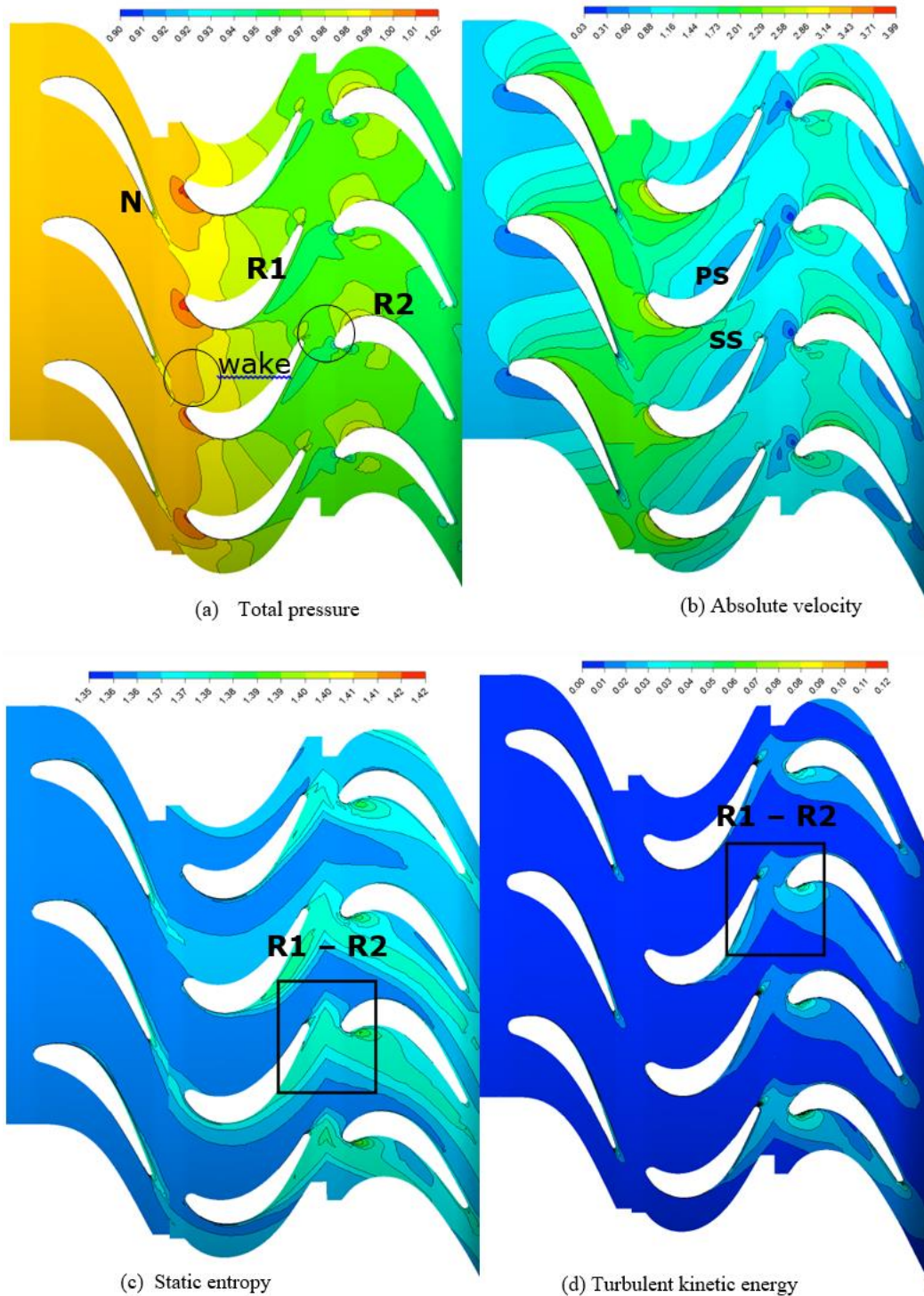


Fig. 8. Blade-to-blade distributions of total pressure, absolute velocity, entropy and TKE.

in Fig. 9 (c). These losses increase as the flow rate is increased.

At the outlet of rotor 1, pressures are not varying from hub-to-tip for low flow rates as shown in Fig. 9 (d). For flow rates of 0.137 and 0.121, increased passage losses tend to decrease total pressures just below the midspan, which is observed at rotor 2 inlet as well, as revealed in Fig. 9 (e). At the exit of

rotor 2, total pressures are similar for all the flow rates throughout the span, except at the tip where tip clearance losses tend to reduce pressure. Thus, there is no distinctive total pressure reduction observed in the nozzle, which just guides the flow. In rotor 1, pressure change from inlet to outlet is more compared to rotor 2 for all the flow rates. Total pressure changes are more as the flow rate is increased beyond 0.108. This pattern is again

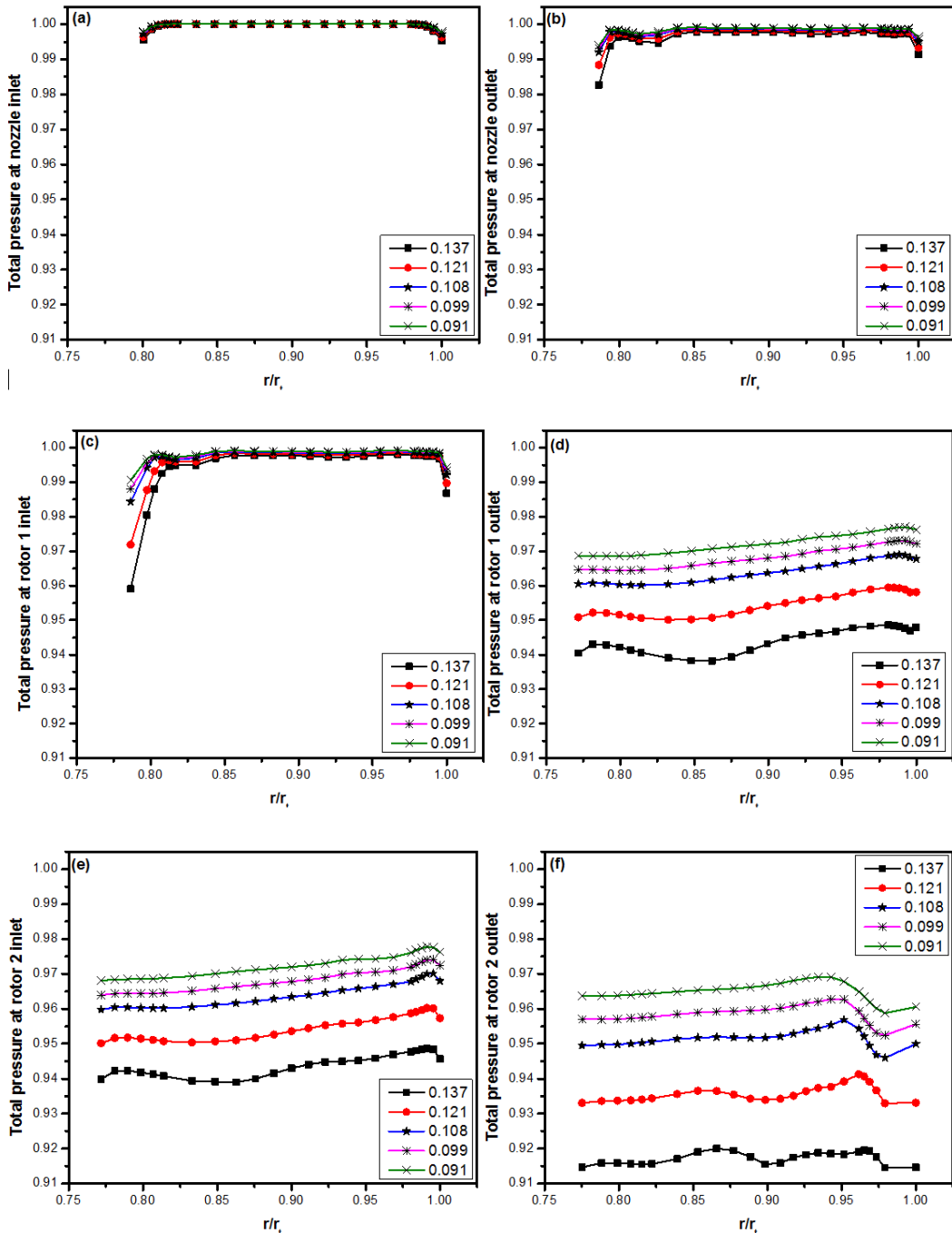


Fig. 9. Total pressure variation in CRT stage from hub-to-tip.

changing from rotor 1 to rotor 2. In rotor 1, total pressure change is more for the highest flow rate. In case of rotor 2, total pressure change at the inlet and outlet is changing more for flow rates above 0.108. Entropy distribution across the span is shown in Fig. 10 for various flow rates. Entropy values remain low, both at the entrance and exit of the stationary nozzle. At nozzle inlet, entropy is not changing with flow rate. Because of the flow losses near the boundary, entropy values are high near the hub and tip at nozzle outlet as shown in Fig. 10 (b). Entropy values slightly increased with flow rate.

Same pattern is observed at the inlet of rotor 1 with change in magnitude, which are more near the hub. At rotor 1 outlet, entropy values are not varying from hub-to-tip for mass flow rates of 0.108, 0.099 and 0.091 as shown in Fig. 10 (d). For the flow rates of 0.132 and 0.121, the entropy values are high from midspan to the tip section which is due to the passage losses that arise in the rotor, which is same at the inlet of rotor 2 as shown in Fig. 10 (e). At the exit of rotor 2, variation of entropy is more for higher flow rates of 0.132 and 0.121, which is clearer from midspan to tip.

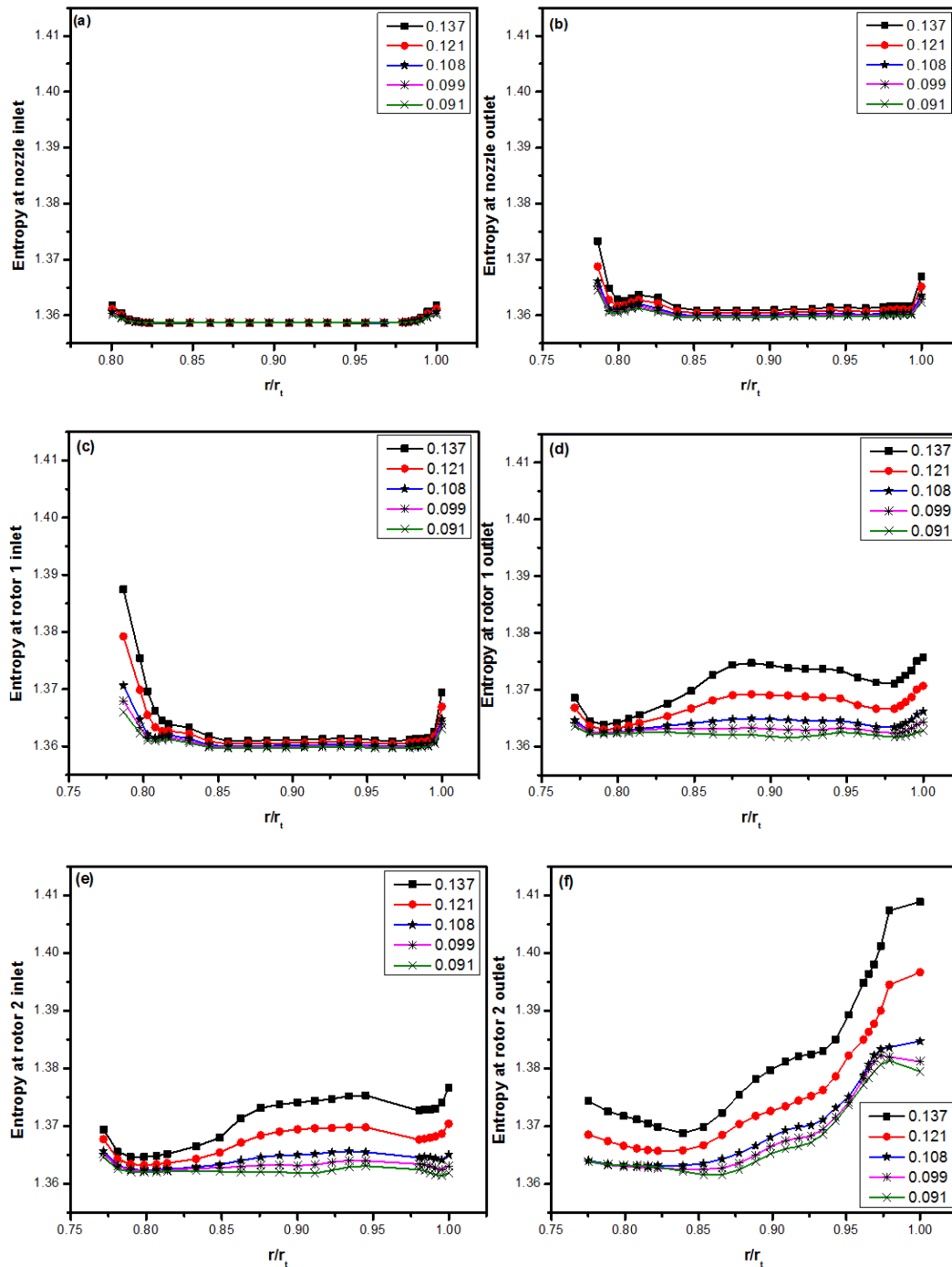


Fig. 10. Entropy variation in CRT stage from hub-to-tip.

5. CONCLUSIONS

Flow characteristics in counter rotating turbine are studied computationally. Contours are drawn on planes along the axial chord and blade-to-blade. Hub-to-shroud distributions and variations on normalized planes are provided for further understanding of the flow physics. Total pressure, axial velocity, entropy and TKE are the parameters used to capture the flow physics through CRT. Total pressure distribution near the midspan in case of nozzle shows the presence of boundary layer and

wake regions. Hub and tip side vortices are also observed at nozzle outlet. In rotor 1, total pressures are highest near the leading edge as the flow from nozzle interacts with rotor 1 with less incidence. On the other hand, for rotor 2, flow impinges on the suction side with incidence. Entropy of nozzle exit flow field is carried to the inlet of the rotor 1 in the form of wake. Secondary flow losses near the hub are also observed at the inlet of rotor 1 passage. TKE contours showed increased flow turbulence from mid-chord region to the outlet as the flow accelerates while travelling to the downstream.

Secondary velocity vectors drawn in rotors 1 and 2 show the presence of tip clearance vortex in the planes before and after the trailing edge. Tip clearance effect is observed to be more in rotor 2 as axial velocities are low near the tip than the rest of the span. Passage vortex observed in rotor 2 is large in size and dominant when compared to the first rotor. Blade-to-blade contours of CRT reveal the actual flow scenario surrounding the blades. These also show clearly that flow is impinging smoothly on rotor 1 and with some incidence on rotor 2. Also, it is revealed that flow losses are more in rotor 2 when compared to rotor 1. Hub-to-tip plots show the variations of flow parameters while moving from the bottom to top most position of blade. Variations near the hub and tip are easily identifiable. Plots and contours drawn along the three directions disclose the actual scenario of wakes, vortices and flow losses. Thus the present work identifies the exact flow structure in a counter rotating turbine. These flow aspects will be useful in adjudging the performance of CRT stage, depending on the application.

REFERENCES

- Dring, R. P., H. D. Joslyn, and M. F. Blair (1987). The effect of inlet turbulence and rotor/stator interactions on the aerodynamics and heat transfer of large scale rotating turbine model. *NASA Report*, CR 179469.
- Ji, L. C., X. B. Quan, L. Wel, and J. Z. Xu (2001). A vaneless counter rotating turbine design towards limit of specific work ratio. *ISABE paper* 2001-1062.
- Louis, J. F. (1985). Axial flow contra-rotating turbines. *ASME paper*, 85-GT-218.
- Moroz, L., P. Pagur, Y. Govorushchenko, and K. Grebennik (2009). *Comparison of counter-rotating and traditional axial aircraft low-pressure turbine integral and detailed performances*. Intl. Symposium on heat transfer in Gas Turbine systems, Antalya, Turkey.
- Ozgun, C., and G. K. Nathan (1971). Study of contra-rotating turbines based on design efficiency. *Journal of Basic Engineering* 93, 395-404.
- Subbarao, R., and M. Govardhan, (2014). Effect of speed ratio on the performance and flow field of a counter rotating turbine. *Journal of Energy Procedia* 54, 580-592.
- Wintucky, W. T., and W. L. Stewart (1957). Analysis of two-stage counter-rotating turbine efficiencies in terms of work and speed requirements. *NACA Report*, RM E57L05.
- Zhao, Q. J., H. S. Wang, X. L. Zhao, and J. Z. Xu (2007). Numerical analysis of 3-D unsteady flow in a vaneless counter rotating turbine. *Frontiers of Energy and Power Engineering in China* 1(3) 352-358.